JTTEE5 5:62-68

Analysis of a High-Velocity Oxygen-Fuel (HVOF) Thermal Spray Torch Part 2: Computational Results

W.L. Oberkampf and M. Talpallikar

The fluid and particle dynamics of a high-velocity oxygen-fuel (HVOF) torch are analyzed using computational fluid dynamic (CFD) techniques. The thermal spray device analyzed is similar to a Metco Diamond Jet torch with powder injection. The details of the CFD simulation are given in a companion paper. This paper describes the general gas dynamic features of HVOF spraying and then discusses in detail the computational predictions of the present analysis. The gas velocity, temperature, pressure, and Mach number distributions are presented for various locations inside and outside the torch. The two-dimensional numerical simulations show large variations in gas velocity and temperature both inside and outside the torch due to flow features such as mixing layers, shock waves, and expansion waves. Characteristics of the metal spray particle velocity, temperature, trajectory, and phase state (solid or liquid) are also presented and discussed. Particle velocities and temperatures are shown to be lower for this type of torch than previously believed.

1. Introduction

NUMERICAL simulations for thermal spraying have grown in sophistication over the last few years. This improved mathematical modeling of the complex physics in thermal spraying has been made possible by both improved numerical methods and the application of computational techniques developed for liquid and solid rocket motors. Axisymmetric and planar two-dimensional computational fluid dynamic (CFD) simulations of chemically reacting, dissociated and ionized flow and of two-phase flows, along with state-of-the-art turbulence models, have been presented by various researchers. For a complete review of the literature regarding numerical simulations of thermal spraying, see the companion paper in this volume (Ref 1).

This paper describes the general gas dynamic features of HVOF spraying and then details the numerical predictions of a CFD analysis. The companion paper (Ref 1) presents the detailed formulation and numerical methods of the present CFD analysis. The HVOF torch analyzed is similar to the Metco Diamond Jet torch, but certain simplifying assumptions have been made. The gas velocity, temperature, pressure, and Mach number distributions are presented for various locations inside and outside the torch. Characteristics of the metal spray particle velocity, temperature, trajectory, and phase state (solid or liquid) are also presented and discussed. Extensive flow visualization is provided to show flow features such as mixing layers, shock waves, and expansion waves.

Keywords computational fluid dynamics, gas dynamics, HVOF, numerical analysis, particle dynamics

W.L. Oberkampf, Aerosciences and Compressible Fluid Dynamics Department, Sandia National Laboratories, Albuquerque, NM 87185-0825, USA; and **M. Talpallikar,** CFD Research Corporation, Huntsville, AL 35805, USA.

2. General Flow Field Characteristics

2.1 *Internal Flow*

Various types of HVOF thermal spray torches have different means of introducing the material to be sprayed and the fuel and oxygen. Each design produces distinct gas dynamic, combustion, heat transfer, and particle dynamics characteristics. The geometry chosen for the present analysis is similar to the Metco Diamond Jet torch, but there are notable differences. Figure 1 shows the internal geometry of the conceptual, axisymmetric torch analyzed. Reference 1 gives a detailed description of the torch geometry and inlet flow characteristics.

The central stream of argon and particles is typically injected at room temperature and at low velocity, with a Mach number of less than 0.1. The oxypropylene and air streams are injected at higher speeds, with a Mach number in the range of 0.3 to 0.6, depending on the mass flow settings for the gases. The Mach number of the incoming streams also depends on the operating pressure inside the aircap. Because the incoming streams are subsonic, the pressure at the exit of the nozzle channels must match the pressure inside the aircap near the incoming streams. If the aircap is removed and the mass flow rate is held constant, the oxypropylene jets become supersonic because the ambient pressure is reduced compared with the aircap operating pressure.

The release of thermal energy from the oxypropylene combustion increases pressure inside the aircap to the degree that the flow chokes at the exit. If the torch is not ignited—that is, if combustion does not occur—the total mass flow rate of the various gas streams is not sufficient to choke the flow at the exit of the aircap. Once the torch is ignited, the torch remains lit because of the separated flow regions formed at the face of the nozzle. These separated, or reversed, flow regions serve as a flame holder for hot combusting gases to ignite the incoming fuel/oxygen stream. The characteristics of these separated flow regions

are very similar to those of the flow near the injector head of a rocket engine and the base region of rocket-powered missiles. If these separated flow regions are eliminated, the torch will not stay lit because the flame speed is much less than the incoming fuel/oxygen gas speed. The reaction zone, or flame front, spreads across the premixed oxypropylene stream as it mixes with the air and argon/particle streams. Note that this ignition characteristic of the premixed oxyfuel stream is not in the present reacting flow model. As discussed in Ref 1, the present model assumes an approximate chemical equilibrium model. This results in an infinite reaction rate, essentially a detonation, of the fully mixed streams as soon as they enter the computational domain.

Near the face of the nozzle, four free-shear layers exist between the mixing streams: one between the argon/particle stream and the adjacent nozzle base flow, two between the oxypropylene stream and the nozzle base flow (one on each side of the oxypropylene stream), and one between the air stream and the nozzle base flow. In addition, the air stream continues to form a boundary layer, that is, an attached shear layer with the aircap wall. Under normal operating conditions, each of these shear layers is turbulent along with the incoming streams.

2.2 *External Flow*

The pressure in the aircap is sufficient to choke the flow through the aircap exit; Mach one is attained at the exit of the aircap. Because the pressure in the exit plane is typically greater than the ambient condition, the aircap flow is said to be underexpanded. The flow will expand supersonically, external to the aircap, so as to meet the ambient pressure condition. The external pressure adjustment of the supersonic stream occurs through an alternating series of expansion and compression waves. Figure 2 shows a simplified depiction of the expansion, compression, and shock waves in the supersonic jet along with the free-shear layer, or mixing layer, surrounding the jet. The angle of the expansion and compression waves with respect to the local gas velocity is known from fundamental gas dynamics to be $\sin^{-1}(1/M_l)$, where M_l is the local Mach number.* If it is assumed that the flow is uniform in the exit plane and the Mach number is unity, the first wave emanating from the edge of the exit is at an angle of 90°. The angle of the last wave is determined by the Mach number to which the flow must expand to decrease the pressure to the ambient conditions. The pressure in the outer portion of the mixing layer is constant at a value equal to the ambient pressure. To simplify the wave pattern in Fig. 2, the waves are shown as straight lines; in reality they are curved, because the local Mach number varies across the stream.

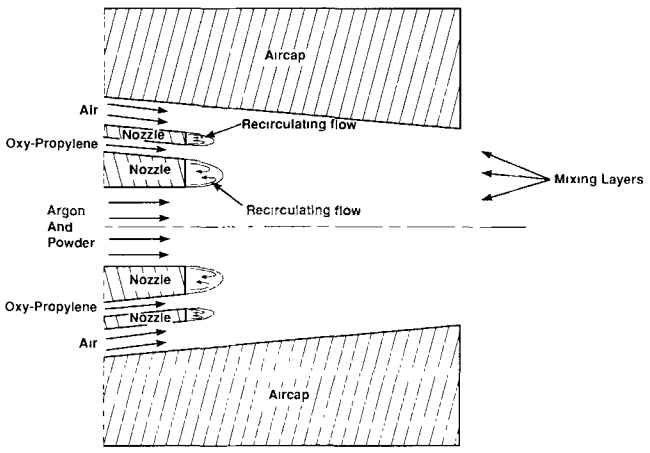

Fig. 1 Mixing layers and separated flows inside the HVOF torch

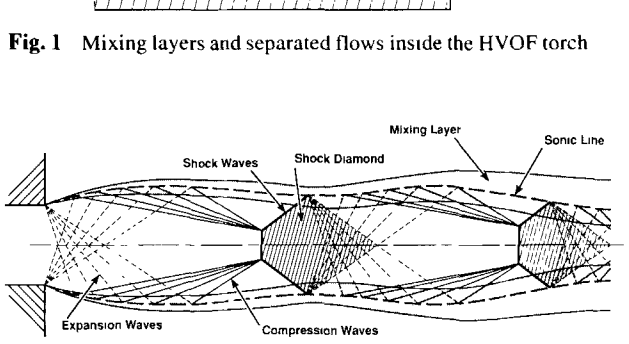

Fig. 2 Mixing layer and wave structure in a supersonic underexpanded jet

The expansion waves intersect the mixing layer on the periphery of the jet and penetrate the mixing layer to the sonic line (Fig. 2). The turbulent mixing layer is a region of large velocity gradient where the flow changes from supersonic speeds to near-zero velocity in the ambient flow. After the expansion waves intersect the mixing layer, they are reflected as compression waves, since waves in supersonic flow reverse character when they intersect a constant-pressure boundary (i.e., a free-jet boundary). The compression waves coalesce into a normal shock wave near the centerline and into an oblique shock wave near the mixing layer. Whether a normal shock or an oblique shock occurs near the centerline depends on the strength of the compression waves. For ratios of exit plane pressure to ambient pressure greater than roughly 2, a normal shock occurs near the centerline of the shock diamonds. For pressure ratios of less than about 2, but yet supersonic flow, an oblique shock wave occurs near the centerline. The condition where all the shock wave reflections are oblique is referred to as "regular wave reflection." The condition where the normal shock wave occurs near the centerline is referred to as "Mach reflection."

The shock waves raise the temperature of the gas such that certain gas species luminesce. These high-temperature, embedded regions are normally referred to as "shock diamonds." The oblique shock wave intersects the free-shear layer and reflects as a "fan" of expansion waves. This expansion fan nearly duplicates the original expansion fan originating from the corner of the exit plane of the aircap. If viscosity did not exist (i.e., assuming inviscid flow), the series of expansion/compression/shock waves would repeat indefinitely. Because of viscosity, however, the mixing layers eventually meet on the centerline of the jet after several shock diamonds. The length of the visible shock-diamond plume indicates the longitudinal extent of the supersonic flow. The supersonic flow eventually decays to subsonic conditions throughout the jet while entraining increasing amounts of cool ambient air (Ref 2).

*The local Mach number is the ratio of the local velocity to the local speed of sound. The Mach number is not a velocity, but rather a scaled, or normalized, velocity.

3. Computational Results

3.1 *Internal Flow Field*

Figure 3 shows the computed static temperature distribution inside the aircap using shaded contours. Recall that the premixed oxypropylene stream enters from the nozzle between a radial position of 2.5 to 3 mm. This can be seen as the very small region of cool gas (313 K) entering from the nozzle on the left. The chemistry model includes nine gas species: C_3H_6, O_2, CO_2, CO, H, H_2, H_2O, O, and OH. The model takes into account the dissociation of the gaseous combustion products. If dissociation of the gases is not included in the chemistry model, then the predicted temperatures will be unrealistically high, roughly by a factor of two for the present fuel and oxygen reactants. The peak combustion temperature for the present simulation is 3100 K, which is slightly higher than the equilibrium chemistry calculation of Power et al. (Ref 3) for a similar torch and comparable gas flow rates. The chemistry model also assumes instantaneous reaction of the premixed oxypropylene stream as soon as it enters the computational domain. Physically, this implies that the combustion energy (i.e., enthalpy) is released in the first line of computational cells near the oxypropylene inlet. This results in a "detonation" of the premixed fuel and oxygen in the computational domain. An improved chemistry model would use finite-rate chemistry to model the gradual ignition of the oxyfuel stream over a finite axial distance. Although this model would provide a more realistic energy release process, computational time for a solution would increase by roughly a factor of two to ten, depending on the complexity of the chemistry model.

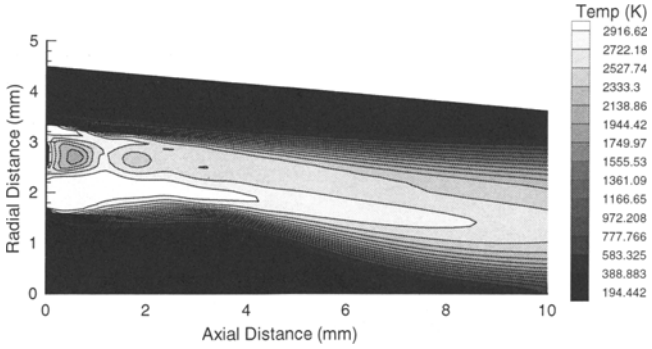

Fig. 3 Temperature contours inside the aircap

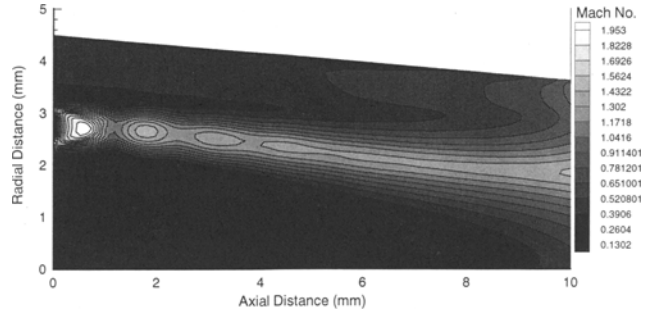

Fig. 4 Mach number contours inside the aircap

As can be seen in Fig. 3, the high temperatures persist in the core of the combusting oxypropylene jet through most of the length of the aircap. At the exit plane the peak temperature is 2600 K. The combusting jet mixes moderately with the argon/particle stream, primarily because it is directed 5° inward toward the centerline. Because of the low mixing, the temperature near the centerline at the exit of the aircap is only 600 K. Very little mixing of the combustion gases occurs with the air stream near the aircap wall. This computationally demonstrates the effectiveness of the air-cooling technique for the aircap.

The Mach number contours inside the aircap are shown in Fig. 4. Recall that the local Mach number is the ratio of the local gas velocity to the local speed of sound and that the local speed of sound is proportional to the square root of the local static temperature. The rapid release of energy near the oxyfuel inlet causes a factor of ten increase in temperature, resulting in a factor of ten decrease in density. This generates high velocities and supersonic flow near the inlet, as if the entering oxyfuel stream were an underexpanded supersonic jet. This supersonic jet goes through expansions, compressions, and shock diamonds just as the underexpanded supersonic jet discussed in section 2.2. Although the supersonic jet characteristic is a result of the chemical equilibrium assumption, this characteristic would not occur in reality because of finite-rate reactions. If all chemical reactions occur inside the aircap, however, the present equilibrium model should produce qualitatively correct Mach numbers and velocities inside and outside the aircap.

Because of the three coaxial streams, with one reacting, the flow is extremely nonuniform at the exit of the aircap. One-third of the exit plane flow (near the centerline) is subsonic. The middle third of the flow annulus is supersonic, with a peak Mach number of 1.4. The outer third annulus is a nearly uniform sonic flow. This presents a much more complex stream for expansion than discussed in section 2.2 (Fig. 2). There, the Mach number of the underexpanded jet was unity all across the exit plane, and the velocity and temperature were uniform.

Figure 5 shows the axial velocity component versus radial position for x = 3, 6, and 9 mm from the face of the nozzle. This plot clearly shows the development of the velocity profiles through each of the three coaxial streams, including the mixing layers between each stream. The thickness of the turbulent boundary layer on the aircap wall can be seen as the sharp decrease in velocity near the wall. The boundary layer thickness is

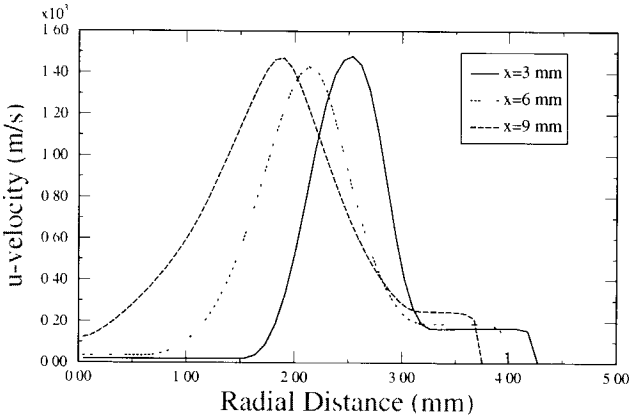

Fig. 5 Axial velocity profiles inside the aircap

roughly 0.15 mm. The peak velocity of the combustion gases remains nearly constant, away from the oxyfuel inlet, at a value of 1500 m/s. Mixing of the high-velocity combustion gases with the argon/particle streams is more effective than with the air cooling layer, because the oxyfuel stream is directed inward and the core flow is at a lower velocity. Because of the radius of the core flow, however, the velocity on the centerline near the exit of the aircap (x = 9 mm) is only 160 m/s.

Contours of the computed (static) pressure distribution inside the aircap are shown in Fig. 6. This plot shows that the pressure in the aircap is essentially constant, except for large variations near the inlet of the oxypropylene stream and near the exit of the aircap. The expansion and compression regions associated with the supersonic combusting jet are also seen in the pressure contours. Away from the jet, however, the pressure over the majority of the aircap is at a constant value near 250 kPa absolute (2.5 atm). As the flow nears the exit plane, the pressure begins to decrease as the flow accelerates. Correct prediction of pressure levels in the aircap is important to the validation of the CFD simulations. Since the flow in the aircap is choked primarily because of the energy release from combustion, correct prediction of pressure is an indication of the combustion modeling accuracy. The CFD analysis of Power et al. (Ref 3, 4) using a similar torch geometry and gas flow rates yielded a pressure of 3 atm. Future related work on HVOF spraying will measure the pressure at different locations inside the aircap and for various operating conditions. These measurements will then be compared to CFD predictions for matching torch geometry and flow rates.

3.2 *External Flow Field*

Figure 7 shows the absolute (static) pressure on the centerline of the torch versus axial distance. This plot clearly shows the magnitude of the pressure changes due to the expansion and compression waves intersecting the centerline flow exterior to the aircap. The pressure decreases from 200 kPa (2.0 atm) in the exit plane of the aircap (x = 10 mm) to a minimum of 50 kPa at the maximum influence of the expansion waves. The first shock wave—that is, the beginning of the first shock diamond—begins at about 17 mm and then compresses the flow to roughly 130 kPa. This pattern can be seen repeating itself such that three, or possibly four, shock diamonds can be identified before the flow stabilizes at atmospheric pressure. As will be seen later, the flow on the centerline at the exit of the computational domain is near a Mach number of unity.

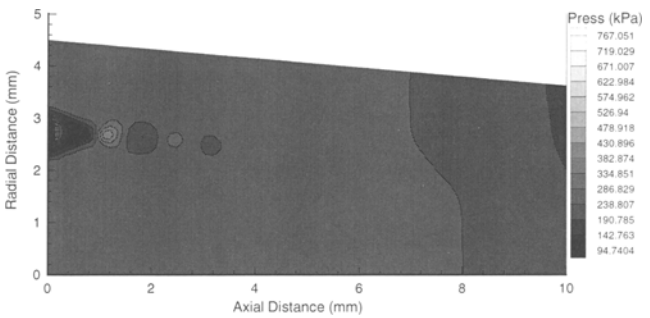

Fig. 6 Static pressure contours inside the aircap

Contours of gas temperature over the entire computational domain are shown in Fig. 8. Three of the four shock diamonds noted in Fig. 7 are visible as regions of elevated temperature in this contour plot. In a previous section, a qualitative description was given of the structure of an underexpanded supersonic jet. That description, however, assumed uniform, Mach one flow at the exit of the aircap. As one would suspect from the previous internal flow description and these temperature contours, the HVOF jet structure will be much more complex. For example, Fig. 8 suggests that the plume would have two distinctive characteristics. First, the gas luminosity near the centerline before the first shock diamond should be significantly less than the surrounding gas because it would be primarily low-temperature argon. Second, the first shock diamond would have nonuniform luminosity because of the large variation in temperature across the diamond. The luminosity near the center of the first shock diamond would be much less than off the centerline; the diamond would appear to have a hole in the center. This plot also shows the axial distance required for the low-temperature argon carrier gas to be mixed with the surrounding high-temperature stream. By an axial position of about 30 mm, the low gas temperature along the centerline is essentially gone; the peak temperature occurs on the centerline. After this point, the cooling of the HVOF jet by mixing with the ambient air becomes the dominant characteristic.

Figure 9 shows the temperature along the centerline of the torch versus axial distance. This plot exemplifies the complexity of the multiple stream mixing in the HVOF torch being analyzed. This shows that the centerline temperature remains at

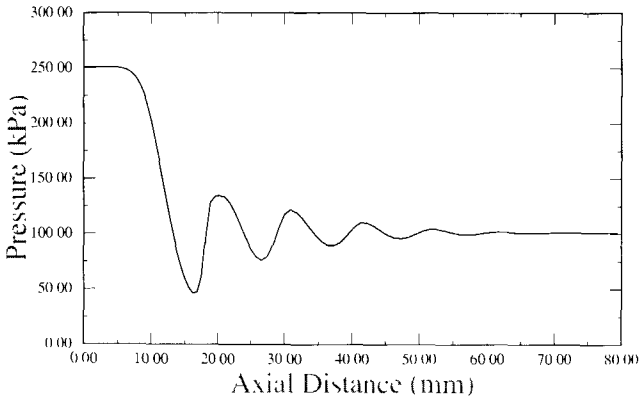

Fig. 7 Static pressure versus axial distance along the centerline

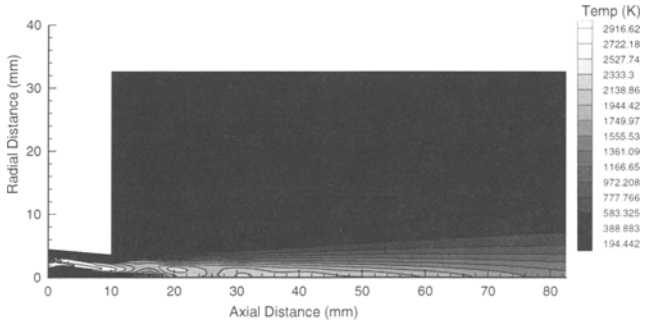

Fig. 8 Temperature contours over the computational domain

room temperature until $x = 9$ mm. The rapid rise in temperature between 9 and 13 mm is due to the combustion gases mixing with the cool argon/particle stream. Over this same distance, however, the flow surrounding this core flow is expanding supersonically; that is, the surrounding gas temperature is decreasing. This characteristic becomes dominant between 13 and 17 mm, where the temperature decreases due to supersonic flow expansion. As mentioned earlier, the first shock diamond begins at 17 mm, and this compression increases the gas temperature. Shock heating combines with the increase in temperature due to combustion gas mixing to cause a continued increase in temperature.The second expansion region begins at 21 mm and causes a drop in temperature, overpowering the increase in temperature due to mixing. After 30 mm, two more weak expansion and compression regions cause the temperature to oscillate, but with decreasing amplitude. After 50 mm, the centerline temperature monotonically decreases due to mixing with the cool ambient air.

The axial velocity of the gas (u-component of velocity) vs. radius for axial locations of 10, 25, 50, and 75 mm is shown in Fig. 10. At the exit of the aircap, $x = 10$ mm, the velocity varies from 200 m/s on the centerline to 1550 m/s in the center of the combusting stream. This factor of eight variation in velocity shows the importance of analyzing these types of HVOF torch designs using two-dimensional CFD techniques instead of one-dimensional flow analyses. One-dimensional analyses assume fully mixed flow at each axial station and thus are unable to capture the required flow physics. Also seen at $x = 10$ mm is the sharp decrease in velocity through the turbulent boundary layer near the wall of the aircap ($r = 3.62$ mm). At $x = 25$ mm, the ratio between the peak velocity and the centerline velocity has decreased to 1.8. The gas velocity on the centerline (1000 m/s) peaks at $x = 20$ mm, and the peak velocity in the combusting stream (1660 m/s) occurs near the same location. Near the end of the computational domain, $x = 75$ mm, the velocity deficit on the centerline has essentially disappeared. From this point on, the decay of the velocity profiles are similar to those from a hot jet with uniform velocity at the exit plane. Preliminary laser velocimetry measurements by Neiser et al. (Ref 5) on the centerline of a similar torch geometry, operating at comparable conditions, have yielded gas velocities near the present predictions.

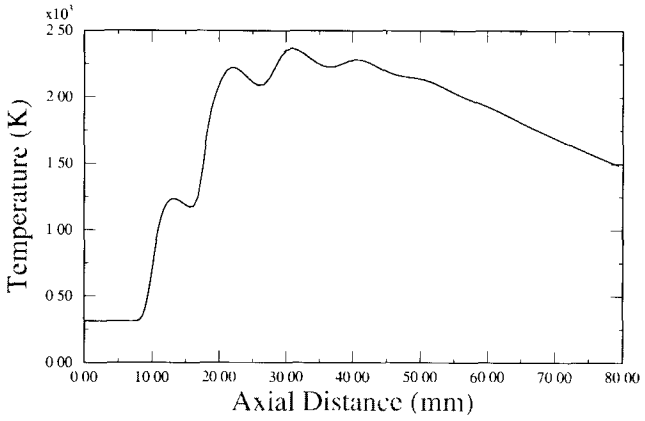

Fig. 9 Temperature versus axial distance along the centerline

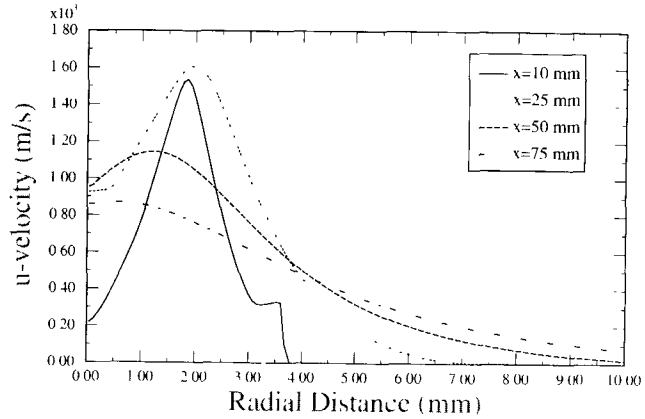

Fig. 10 Axial velocity profiles outside the aircap

Figure 11 shows the contours of local Mach number for the torch. It is clearly seen that an annulus of supersonic flow persists even through the compression waves associated with the shock diamonds. The peak Mach number in this annulus is roughly 1.9. In the center of the stream, however, the jet is subsonic until $x = 13$ mm, at which point it attains Mach one. Continued mixing of the core flow and also the supersonic expansion waves result in a peak Mach number on the centerline of 1.6 at $x = 17$ mm. After this point, the normal shock wave near the centerline causes the Mach number to become subsonic (0.4) at 20 mm. The flow accelerates after the shock diamond and becomes supersonic again, and is processed by two more compressions and expansions. It is also noted in Fig. 11 that the flow near the centerline at the outflow boundary of the computational domain is supersonic, M = 1.1. The centerline Mach number decreases very slowly for $x > 60$ mm. In this region, the local velocity decreases, but the local speed of sound also decreases due to the cooling of the jet. This results in a nearly constant Mach number.

3.3 *Particle Characteristics*

The 30 μm copper particles are assumed to be uniformly dispersed in the argon gas flow in the center stream of the nozzle. Specific initial locations of particles must be chosen so as to track the motion of the particles through the aircap and into the external flow field. To obtain representative results for particles, eight computational, or tracker, particles were introduced into the argon stream. Each of these computational particles represents a large number of actual copper particles in the stream. The

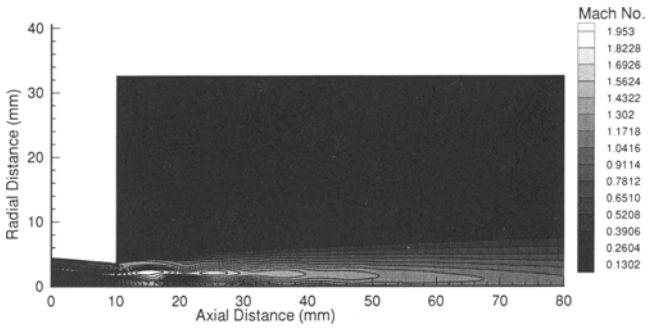

Fig. 11 Mach number contours over the computational domain

initial locations of computational particles are chosen to be evenly distributed across the incoming argon stream. Recall from the computational formulation (Ref 1) that the particles are assumed to be at the same temperature and velocity of the argon at injection. Figure 12 shows the trajectory of each of the eight computational copper particles. Note that the radial scale is greatly expanded, roughly by a factor of 30, to show the small radial motion of the particle trajectories. Outside the aircap, the simulation predicts all particles are within 0.7 mm of the centerline at $x = 80$ mm. Because of the complex interaction of particles with turbulent eddies in the gas, which is not in the present simulation, it is believed that some particles will be dispersed farther from the centerline than the present simulation predicts.

Although the particles are introduced across the argon stream, up to 1.5 mm from the centerline, the 5° radial component of velocity in the oxypropylene and air streams moves all of these particles to within 0.7 mm of the centerline. An interesting feature of the trajectories is the apparent "bouncing" of two of the particles on the centerline, one near 43 mm and one near 58 mm. The CFD code computes any impact of a solid particle on a surface as a specular reflection. Although the centerline is not a surface, it is a line of mirror symmetry in axisymmetric flow. As a result, the computational interpretation of the "bouncing" of the particles is simultaneous impact of particles with their mirror image from the opposite side of the line of symmetry. Reinterpreting the computational "bouncing," one can conclude that the reflection is, physically, a particle traversing from the opposite side of the torch.

Figure 13 shows the temperature of each of the eight particles versus axial position. Also shown in the plot is the temperature of the gas on the centerline, since the particles are near the centerline. The particles show a range in temperatures, depending on where they were introduced into the argon stream. Particles near the edge of the argon stream are exposed to the highest gas temperatures because of the mixing layer with the combustion stream. It can be seen that the two particles near the edge of the argon stream are the only particles that attain the melting temperature of pure copper, 1358 K. These two computational particles, however, have not absorbed sufficient heat to fully melt the particles. They are 20% and 8% melted, respectively, when they exit the computational domain. Because the gas temperature at the edge of the computational domain has nearly dropped to the particle melt temperature, it can be concluded that none of the copper particles will fully melt.

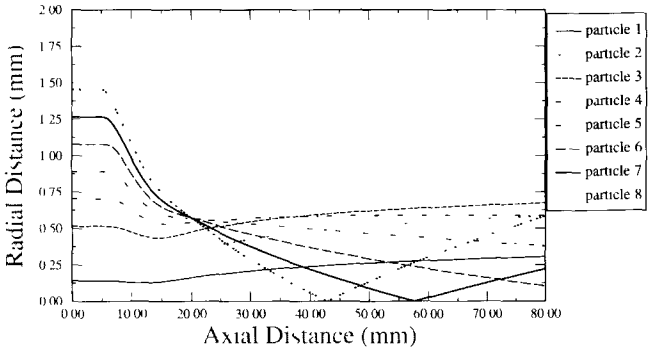

Fig. 12 Particle trajectories

Predicted particle velocities versus axial position, along with the velocity of the gas on the centerline, are shown in Fig. 14. At the exit of the aircap, the velocity of the particles ranges from 20 to 60 m/s, depending on their location when introduced into the argon stream. As was discussed earlier, the explanation for the low particle velocities at the aircap exit is the very low gas velocities near the centerline in the aircap (see Fig. 5 and 10). Outside the aircap, the particles steadily increase in speed, although their velocities are not as high as is commonly experienced for HVOF spraying. As the particles exit the computational domain, they are predicted to be in the range of 220 to 240 m/s. Preliminary particle velocity measurements by Neiser et al. (Ref 5) are near the unexpectedly low values predicted by the present analysis.

An interesting feature to note from the particle velocities is their response to the expansion waves and shock waves in the jet. Small particles—for example, less than 1 μm—respond rapidly to changes in velocity, but large particles tend to be unresponsive. From Fig. 14, the most rapid acceleration of the particles occurs in the region from 11 to 17 mm. This is a result of both the elimination of the velocity defect near the centerline and the supersonic expansion of the flow outside the aircap. Recall from Fig. 11 that Mach one on the centerline occurs at 13 mm. The beginning of the first shock diamond is at $x = 17$ mm, and Fig. 14 shows that there is minimal response of the particle to the shock wave. The velocity slope begins to change at this point. The particles continue to accelerate through the shock diamond, but their rate of velocity increase diminishes. This behavior occurs because the particle velocity is still less than the subsonic gas velocity. After the first shock wave, the influence of the shock diamonds on the particle velocity is not noticeable,

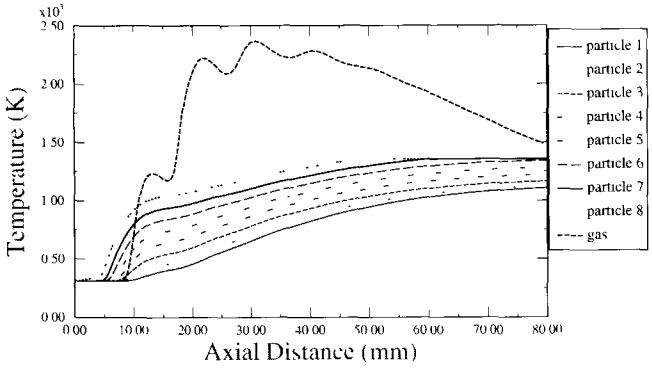

Fig. 13 Particle temperatures versus axial distance

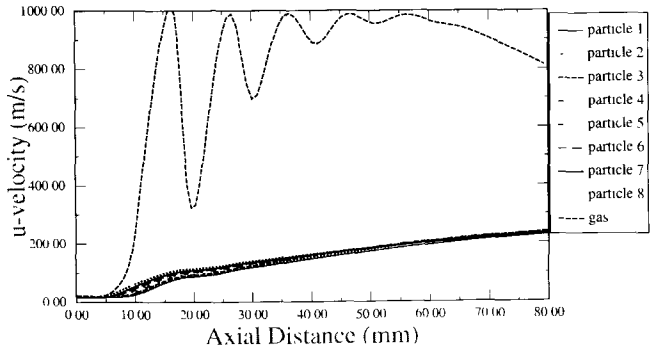

Fig. 14 Particle velocities versus axial distance

because the magnitude of the velocity change through the shock waves steadily decreases as more waves occur.

4. Summary and Future Work

This paper describes the gas and particle dynamics features that exist inside and outside a Metco-type HVOF thermal spray torch. Quantitative numerical results from the computational fluid dynamics modeling are given and discussed. The gas velocity, temperature, pressure, and Mach number distributions are presented for various locations inside and outside the torch. The two-dimensional numerical simulations show large variations in gas velocity and temperature both inside and outside the torch due to flow features such as mixing layers, shock waves, and expansion waves. Characteristics of the metal spray particle velocity, temperature, trajectory, and phase state (solid or liquid) are also presented and discussed. Particle velocities and temperatures are shown to be lower for this type of torch than previously believed.

Future computational work will include development of a finite-rate chemical reaction model. This type of combustion model should improve the prediction of the flow velocities and gas pressures inside the aircap. Although the present instantaneous chemistry model yields the correct energy added to the flow field, its detonation-type release near the nozzle is unrealistic. The detrimental effects of the present combustion modeling can be better judged by comparing it with results from a finite-rate chemistry model and experimental measurements. Also planned in future work is the measurement of pressures inside the aircap and gas and particle velocities outside the aircap. These measurements are critical to building confidence in the present mathematical and numerical modeling.

Acknowledgments

We would like to thank Fritz Owens and Anantha Krishnan of CFD Research Corporation for their technical assistance and consultations. We also thank Amalia Lopez, Rich Neiser, and Mark Smith of Sandia National Laboratories for their technical discussions and generous assistance. Part of this work was performed at Sandia National Laboratories, which is operated by Martin-Marietta Corporation for the U.S. Department of Energy under contract No. DE-AC04-94AL85000.

References

1. W.L. Oberkampf and M Talpallikar, Analysis of a High-Velocity Oxygen-Fuel (HVOF) Thermal Torch, Part 1. Numerical Formulation, *J. Therm. Spray Technol.*, Vol 5 (No 1), 1996
2. C M Hackett, G.S. Settles, and J D. Miller, On the Gas Dynamics of HVOF Thermal Sprays, *Thermal Spray Coatings: Research, Design and Applications,* C.C. Berndt and T.F Bernecki, Ed., ASM International, 1993, p 167-172
3. G.D. Power, T J. Barber, and L M. Chiappetta, "Analysis of a High-Velocity Oxygen-Fuel (HVOF) Thermal Torch," AIAA Paper No 92-3598, presented at AIAA/SAE/ASME/ASEE 28th Joint Propulsion Conf (Nashville, TN), July 1993
4. E B Smith, G D Power, T.J. Barber, and L.M Chiappetta, Application of Computational Fluid Dynamics to the HVOF Thermal Spray Gun, *Thermal Spray: International Advances in Coatings Technology,* C C. Berndt, Ed., ASM International, 1992, p 805-810
5. R.A. Neiser, T J Roemer, and M F Smith, private communication, Sandia National Laboratories, Albuquerque, NM, Oct 1993